environmental microbiology

Environmental Microbiology (2020) **22**(1), 343–353 doi:10.1111/1462-2920.14851

Energy flux controls tetraether lipid cyclization in *Sulfolobus acidocaldarius*

Alice Zhou,[1*†] Yuki Weber,[2] Beverly K. Chiu,[1] Felix J. Elling,[2] Alec B. Cobban,[1] Ann Pearson[2] and William D. Leavitt [1,3,4*]

[1]*Department of Earth Sciences, Dartmouth College, Hanover, New Hampshire, 03755, USA.*

[2]*Department of Earth & Planetary Sciences, Harvard University, Cambridge, Massachusetts, 02318, USA.*

[3]*Department of Chemistry, Dartmouth College, Hanover, New Hampshire, 03755, USA.*

[4]*Department of Biological Sciences, Dartmouth College, Hanover, New Hampshire, 03755, USA.*

Summary

Microorganisms regulate the composition of their membranes in response to environmental cues. Many Archaea maintain the fluidity and permeability of their membranes by adjusting the number of cyclic moieties within the cores of their glycerol dibiphytanyl glycerol tetraether (GDGT) lipids. Cyclized GDGTs increase membrane packing and stability, which has been shown to help cells survive shifts in temperature and pH. However, the extent of this cyclization also varies with growth phase and electron acceptor or donor limitation. These observations indicate a relationship between energy metabolism and membrane composition. Here we show that the average degree of GDGT cyclization increases with doubling time in continuous cultures of the thermoacidophile *Sulfolobus acidocaldarius* (DSM 639). This is consistent with the behavior of a mesoneutrophile, *Nitrosopumilus maritimus* SCM1. Together, these results demonstrate that archaeal GDGT distributions can shift in response to electron donor flux and energy availability, independent of pH or temperature. Paleoenvironmental reconstructions based on GDGTs thus capture the energy available to microbes, which encompasses fluctuations in temperature and pH, as well as electron donor and acceptor availability. The ability of Archaea to adjust membrane composition and packing may be an important strategy that enables survival during episodes of energy stress.

Received 17 August, 2019; revised 16 October, 2019; accepted 22 October, 2019. *For correspondence. E-mail william.d.leavitt@dartmouth.edu; Tel. (+1) 603 646 2978. alice.zhou.gr@dartmouth.edu; Tel. (+1) 408 598 6705. †Present address: Department of Earth and Environmental Sciences, University of Michigan, Ann Arbor, MI 48109, USA.

Introduction

Membrane lipids synthesized by microbes from the domain Archaea can be preserved in sediments for millions of years and are used to reconstruct the past environmental conditions. Isoprenoid lipids known as glycerol dibiphytanyl glycerol tetraethers (GDGTs) are the main constituents of monolayer membranes in many archaea (Kates, 1993; Koga and Morii, 2007). These membrane-spanning lipids can contain up to eight cyclopentane rings in Cren- and Euryarchaeota, or up to four cyclopentane rings with an additional cyclohexane ring in Thaumarchaeota (Sinninghe Damsté *et al*., 2002). These ring structures enhance lipid-lipid interactions (Gabriel and Chong, 2000; Nicolas, 2005; Shinoda *et al*., 2007a; Shinoda *et al*., 2007b; Pineda De Castro *et al*., 2016), and ultimately, the packing and stability of the membrane (Fig. 1 and Supporting Information Fig. S1). The relative abundance of these ring structures in GDGTs forms the basis for the widely applied sea- (Schouten *et al*., 2002; Schouten *et al*., 2007a) and lake- (Powers *et al*., 2010; Pearson *et al*., 2011) surface paleotemperature proxy known as TEX_{86}.

Membrane-spanning tetraether lipids are the most abundant lipids in many thermophilic archaea (Siliakus *et al*., 2017) and can make up close to 100% of the membranes of acidophilic archaea (Macalady *et al*., 2004; Oger and Cario, 2013). GDGTs were first identified in hyperthermophilic archaea isolated from hot springs with average temperatures >60°C; these lipids were originally interpreted as a primary adaptive feature to high temperatures (De Rosa *et al*., 1974). Pure culture experiments with thermoacidophilic crenarchaeota show that the number of pentacyclic rings in the biphytanyl chains of GDGTs increases systematically with growth temperature (De Rosa *et al*., 1980; Uda *et al*., 2001; Uda *et al*., 2004; Boyd *et al*., 2011; Feyhl-Buska *et al*., 2016). High temperature, however, is not the only challenge to hot spring microbes. Ecosystems that host thermophiles are often characterized by acidity, and archaeal tetraether-based membranes have also been demonstrated to confer

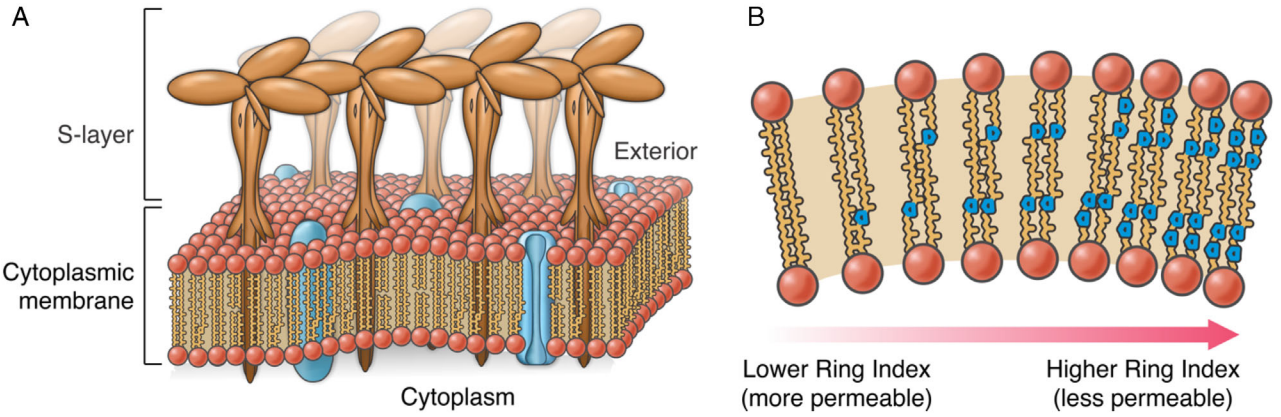

Fig. 1. Schematic of the *Sulfolobus acidocaldarius* cell envelope. A, The cytoplasmic membrane is composed predominantly of monolayer-forming GDGT that are comprised of hydrophobic lipid cores (yellow chains) attached to hydrophilic headgroups (red spheres). The membrane further hosts embedded proteins (blue) and anchors surface-layer (S-layer) glycoproteins, which face the external environment. B, The incorporation of cyclopentyl moieties (blue rings) into the hydrophobic alkyl chains of GDGTs allow the lipids to pack more tightly, decreasing overall membrane permeability.

tolerance to low pH (Macalady *et al*., 2004; Boyd *et al*., 2011; Boyd *et al*., 2013). Archaeal membranes composed of tetraethers are relatively impermeable and thus restrict proton influx into the cytoplasm, allowing cells to better maintain homeostasis at low pH and high temperatures (Elferink *et al*., 1994; Konings *et al*., 2002). GDGTs may be linked to the survival of Archaea at these environmental extremes, and calditol-linked GDGTs were recently shown to be required for growth of *Sulfolobus acidocaldarius* under highly acidic conditions (pH < 3) (Zeng *et al*., 2018). Because these lipids are central to the survival of thermoacidophilic archaea, such organisms are ideal targets to study the role of physicochemical stress on GDGT cyclization.

As a widespread and structurally distinct class of archaeal membrane lipids, GDGTs have been extensively studied with regards to their biophysical properties and role in influencing aggregate membrane behaviour. These lipids form stable, highly impermeable monolayers in which individual lipids have low lateral diffusion rates (Jarrel *et al*., 1998). The incorporation of cyclopentyl rings into these core lipids further increases the thermal stability of membranes. Differential scanning calorimetry experiments on pure lipid films show that thermal transitions are shifted towards higher temperatures as the number of cyclopentane rings increases (Gliozzi *et al*., 1983). The basis for such trends has been illuminated by molecular dynamics simulations across various timescales both *in vacuo* (Gabriel and Chong, 2000) and in solution (Nicolas, 2005; Shinoda *et al*., 2007a; Shinoda *et al*., 2007b; Pineda De Castro *et al*., 2016). These computational studies demonstrate that membranes comprised of highly cyclized GDGTs are more tightly packed, largely due to the more favourable hydrogen bonding interactions that result from the incorporation of cycloalkyl moieties (Gabriel and Chong, 2000; Shinoda *et al*., 2007a). Tight packing causes membranes composed of cyclized tetraether lipids to become more rigid than membranes composed entirely of acyclic GDGTs. The extent of membrane packing exerts control on microbial physiology, as membrane fluidity and permeability directly influence how the cell interfaces with its environment. The closer packing of GDGTs with more pentacyclic rings (Fig. 1) can explain why compositional variations in these lipids are directly linked to experimental or natural gradients in stressors such as temperature (De Rosa *et al*., 1980; Uda *et al*., 2001; Uda *et al*., 2004; Sollich *et al*., 2017) and/or pH (Yamauchi *et al*., 1993; van de Vossenberg *et al*., 1998; Boyd *et al*., 2011; Feyhl-Buska *et al*., 2016),

The ability to survive and grow under conditions of chronic energy limitation may be a defining characteristic of the Archaea (Valentine, 2007). The relative impermeability of archaeal membranes decreases cellular maintenance energy requirements by reducing inadvertent ion diffusion across the cell membrane (Konings *et al*., 2002; Hulbert and Else, 2005), implying that the capacity to vary GDGT composition might be one way to acclimatize to energy limitation. As recently proposed for mesophilic Thaumarchaeota (Hurley *et al*., 2016), if GDGT cyclization plays a role in lowering cellular energy requirements, then limiting the energy flux to a population will result in a measurable effect on cyclization within the biphytanyl cores of membrane GDGTs.

We hypothesize this extends to other GDGT-producing archaea and assess this in a model thermoacidophilic archaeon. In this study, we test the effect of limited electron-donor flux on GDGT cyclization in continuous culture (chemostat) experiments with the heterotrophic thermoacidophile *Sulfolobus acidocaldarius* DSM 639. We restrict feed rates of a limiting substrate, sucrose,

which acts as both the sole carbon source and electron donor. This strategy allows us to set the specific growth rate of the microbial population while maintaining constant temperature, pH, dissolved oxygen, and chemical composition of the growth medium (Novick and Szilard, 1950; Herbert *et al*., 1956). This is the first application of continuous culture work to investigate the effects of energy availability on the lipid composition of a thermoacidophilic archaeon. Our chemostat-based approach pares away the confounding variables associated with batch (De Rosa *et al*., 1980; Uda *et al*., 2001; Uda *et al*., 2004; Boyd *et al*., 2011; Elling *et al*., 2014; Elling *et al*., 2015; Qin *et al*., 2015; Feyhl-Buska *et al*., 2016) and mesocosm (Wuchter *et al*., 2004; Schouten *et al*., 2007) studies, in which metabolic activity and chemical composition change over the course of the experiment and potentially influence lipid distributions.

Results

Lipid distributions and ring indices change in response to electron donor supply

Continuous cultures of the crenarchaeon *S. acidocaldarius* produced GDGTs 0–6 at all growth rates, with the average cyclization (expressed as the Ring Index–RI, see Methods) increasing at longer doubling times (Fig. 2). We observed substantial shifts in the relative abundance of GDGTs with different amounts of cyclopentyl moieties depending on the steady-state growth rates of the cultures (Fig. 2). The mean RI changed from 2.04 $\pm$ 0.06 at the fastest growth rate to 3.19 $\pm$ 0.14 at the slowest growth rate (Fig. 2), corresponding to target turnover rates of 9 to 70 h (see Table 1) and inferred doubling times of 7 to 53 h. Changes in RI were caused by shifts in GDGT distributions, as the relative proportion of GDGTs-4, 5, and 6 increased at slower growth rates (Fig. 2). The RI at each target turnover rate (Table 1) was significantly different from all other rates at a 90% confidence level (two-sample *t*-test, $p < 0.02$), except those targets between and 18 h and 30 h (Fig 3, Supporting Information Figs. S2, S4). To test whether collecting biomass over prolonged intervals altered lipid distributions, a direct comparison between cold trap recovery versus instantaneous reactor biomass was carried out in the slowest target turnover rate (70 h). Neither GDGT distributions nor RI values differed significantly between biomass collected into cold traps versus biomass sampled directly from bioreactors (Fig 3, Supporting Information Fig. S2, S4). Overall, GDGTs were more cyclized at slower reactor turnover times and slower specific growth rates, resulting in higher RI values (Fig. 4, Supporting Information Fig. S5).

Late-eluting GDGT isomers

Small amounts of late-eluting isomers of GDGTs-3, –4, and –5 were observed in all samples (Fig 5 and Supporting Information Fig. S6). These molecules are distinct from the

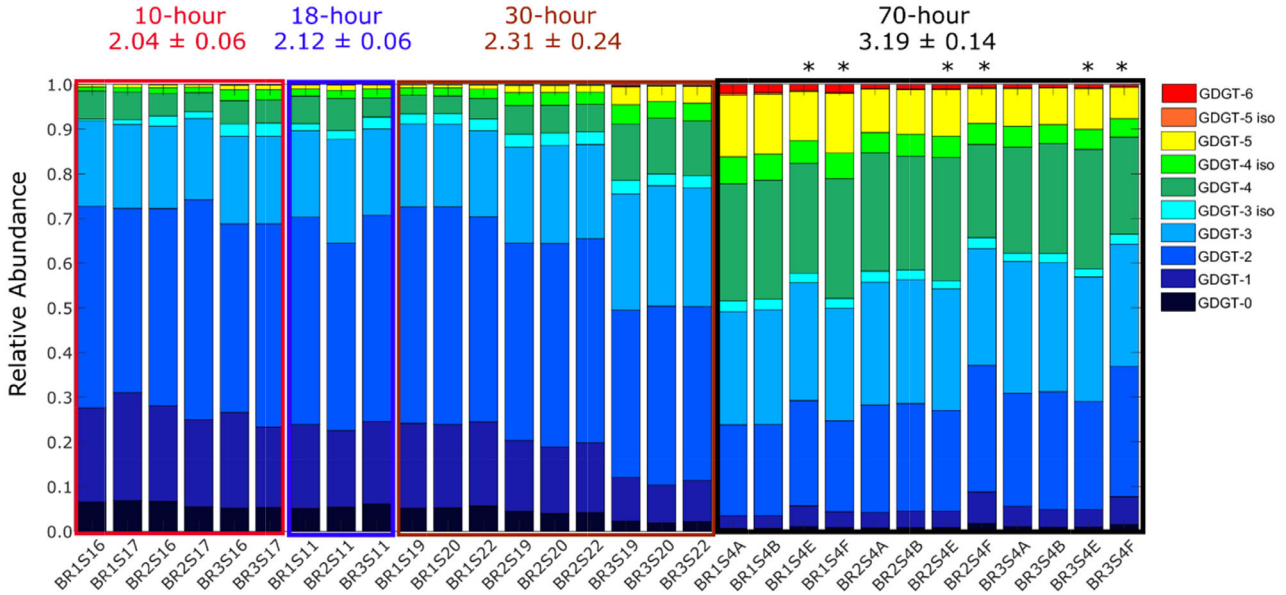

Fig. 2. Relative abundances of core GDGTs change solely as a function of doubling time, which we controlled by fixing the provision rate of sucrose to three independent bioreactors (BR1, BR2 and BR3). At slower growth rates, lipid distributions are shifted toward more highly cyclized GDGTs-4, 5 and 6. The mean and standard deviations for ring index were averaged across all bioreactors for each target turnover rate, noted above the bar chart, as well as the targeted turnover-time for each reactor set (10, 18, 30 or 70 h). Samples denoted with an asterisk (*) were removed directly from reactors; all other samples were generated from biomass collected into ice-chilled reservoirs. Steady state is defined in the Methods.

Table 1. Target and mean turnover times for the four dilution rate experiments, as well as the associated inferred population doubling times at steady state. Values account for small volume changes over the course of the experiment. Intervals in which pumping was interrupted are not included.

	Measured turnover time (h)			Inferred doubling time (h)		
Target turnover time (h)	BR 1	BR 2	BR 3	BR 1	BR 2	BR 3
10	9.2 ± 0.7	9.9 ± 0.4	10.2 ± 0.9	6.9 ± 0.7	7.1 ± 0.9	7.0 ± 0.8
18	17.4 ± 2.3	18.5 ± 3.4	18.0 ± 4.2	12.4 ± 2.1	12.2 ± 2.1	11.9 ± 3.7
30	29.6 ± 0.4	29.9 ± 0.7	31.0 ± 1.6	21.3 ± 4.8	20.4 ± 1.8	21.3 ± 1.4
70	70.2 ± 8.7	62.2 ± 4.6	57.9 ± 4.2	51.6 ± 1.9	41.3 ± 1.2	40.0 ± 1.4

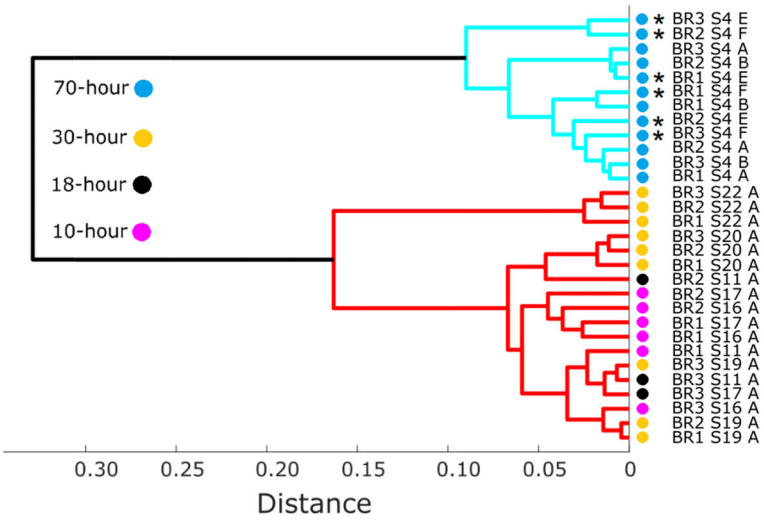

Fig. 3. Average linkage dendrogram (cophenetic correlation coefficient = 0.94) showing dissimilarities between normalized GDGT distributions measured in samples collected from cultures spanning 10 to 70 h target turnover times (n = 3). Asterisks (*) are as in Fig. 2.

early-eluting isomer of GDGT-4 characterized in previous studies (Sinninghe Damsté *et al*., 2012) but may correspond to minor peaks of putative structural isomers observed in *Sulfolobus solfataricus* GDGTs (Hopmans *et al*., 2000). The exact structure of these late-eluting isomers remains unknown. Here, we identified them based on their retention times and molecular masses in relation to the major GDGTs (Supporting Information Fig. S6). In this

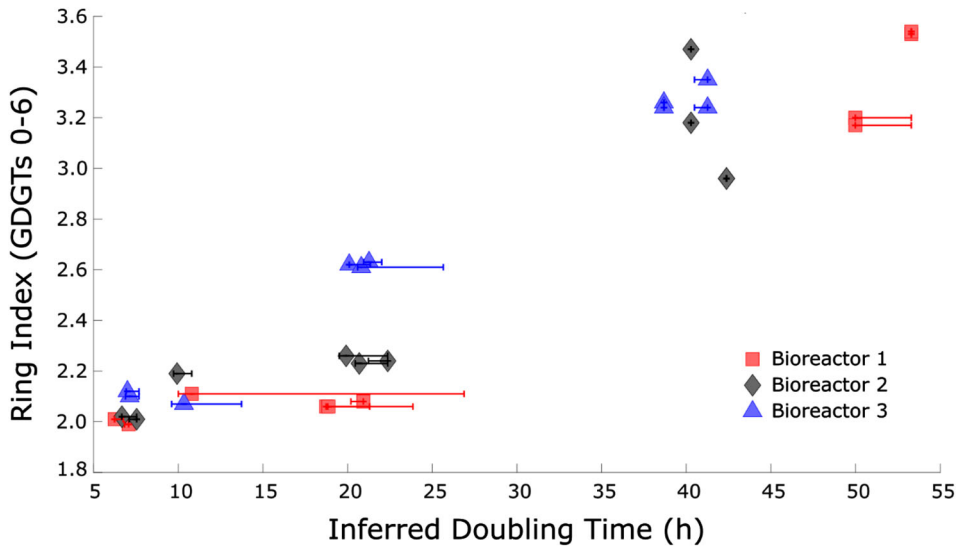

Fig. 4. Core GDGT cyclization increased systematically as a function of doubling times in isothermal continuous cultures of *S. acidocaldarius*. Growth rates are controlled by restricting flux of the limiting substrate (sucrose, which serves as both the sole carbon and electron source). *X*-axis error bars represent the maximum range in inferred doubling times observed during the five reactor turnovers preceding each sampling event.

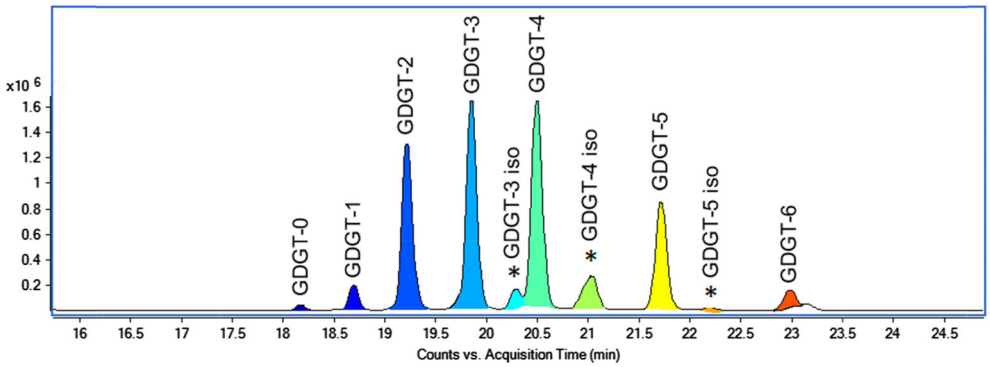

Fig. 5. A representative base peak chromatogram of *Sulfolobus acidocaldarius* core GDGTs, obtained through high-performance liquid chromatography/atmospheric pressure chemical ionization mass spectrometry (HPLC/APCI-MS), showing the positions and peak heights of late-eluting isomers (*) relative to major isomers.

study, the low pH (2.25) may likewise be driving production of late-eluting GDGT isomers. The relative abundances of these isomers were consistent across the entire range of dilution rates tested, which implies that they are not directly involved in a physiological response to energy stress.

Discussion

Ring index is a measure of the average number of cyclopentane rings within an ensemble of GDGTs. Early laboratory work established an empirical relationship between growth temperature and GDGT cyclization in thermoacidophilic Crenarchaeota (De Rosa *et al*., 1980; Uda *et al*., 2001; Uda *et al*., 2004). Liposome experiments and biophysical models demonstrate that this cyclization is associated with an increase in the degree of membrane packing and a coincident decrease in permeability (Jarrel *et al*., 1998; Gabriel and Chong, 2000; Nicolas, 2005; Shinoda *et al*., 2007a; Shinoda *et al*., 2007b; Pineda De Castro *et al*., 2016). While RI is a useful summary metric of archaeal GDGT profiles, it provides a non-unique description of a lipid ensemble. For example, a pure GDGT-3 membrane would have the same RI (3.0) as a membrane that is 50% GDGT-1% and 50% GDGT-5. It is unknown whether membranes composed of those example lipid populations would have identical biophysical properties. As such, it may be an oversimplification to draw conclusions based solely on RI values.

The TEX_{86} ratio is a similar metric that applies to GDGTs produced by marine Thaumarchaeota and is also assumed to be driven by changes in growth temperature (Schouten *et al*., 2002). However, recent pure culture experiments with Thaumarchaeota, Crenarchaeota and Euryarchaeota have shown that other factors significantly alter GDGT distributions, TEX_{86}, and RI. Both mesophilic Thaumarchaeota and thermoacidophilic Crenarchaeota appear to use GDGT cyclization to regulate membrane permeability and fluidity in response to a number of environmental stressors (Uda *et al*., 2001; Macalady *et al*., 2004; Uda *et al*., 2004; Elling *et al*., 2014; Elling *et al*., 2015; Qin *et al*., 2015; Feyhl-Buska *et al*., 2016; Siliakus *et al*., 2017). Specifically, increases in RI during later growth phases in Thaumarchaeota, Crenarchaeota and Euryarchaeota (Elling *et al*., 2014; Jensen *et al*., 2015; Feyhl-Buska *et al*., 2016), and at reduced O_2 concentrations in experiments with Thaumarchaeota (Qin *et al*., 2015), suggest that archaea modulate membrane composition to cope with bioenergetic stress. Since nutrient depletion during later growth phases (in batch cultures) and lower dissolved oxygen results in decreased rates of energy supply, these experiments suggest that there may be a direct feedback between energy availability and cellular membrane composition in GDGT-producing Archaea.

One means to reduce cellular maintenance energy requirements, regardless of surrounding environmental conditions, is to decrease ion permeability across the cytoplasmic membrane (Valentine, 2007). Maintaining a chemiosmotic potential across the membrane is a significant energy expenditure for all living cells, and the spontaneous diffusion of ions across the membrane outside of controlled channels (e.g. ATP synthase) is a form of futile ion cycling that incurs a direct energy loss in the form of reduced membrane potential (Hulbert and Else, 2005; Oger and Cario, 2013). More compact membranes decrease the rate at which ion leakage across the membrane can occur, which will lower cellular maintenance energy requirements. Consistent with this idea, RI should increase at lower energy flux, reflecting an increase in membrane packing under energy limitation. Conversely, RI should decrease as energy availability increases, as the cells would tolerate greater ion leakage. The significant increase in the relative abundance of highly cyclized GDGTs at the slowest sucrose supply rate (Fig. 4) supports the hypothesis that tighter membrane packing is a response to energy limitation and may indicate a physiological response to low-power environments (c.f. Bradley *et al*., 2018).

Clear parallels can be drawn between this study and work with another archaeal taxon. Hurley *et al*. conducted isothermal continuous culture experiments with the mesophilic marine thaumarchaeon *Nitrosopumilus maritimus* SCM1, controlling growth rate by limiting influx of the electron donor, ammonia (Hurley *et al*., 2016). *N. maritimus* is an ammonia oxidizer of direct relevance to the TEX_{86} paleotemperature proxy, and the chemostat-based approach used by Hurley *et al*. constitutes the closest experimental analog to this study. Although *S. acidocaldarius* and *N. maritimus* occupy thermally (T > 60 °C vs. T < 30 °C) and chemically (pH < 3 vs. pH > 7) disparate environments and utilize different carbon and energy metabolisms, they both show a positive correlation between specific growth rate and ring index (Fig. 6). For both taxa, RI increased with doubling time (Fig. 6), although the relative change in average cyclization between end-member growth rates is more pronounced in *S. acidocaldarius* (m = 0.036) than in *N. maritimus* (m = 0.008). This agreement implies that membrane dynamics and cellular bioenergetics are tightly coupled in Archaea.

A full and mechanistic understanding of how Archaea regulate GDGT distributions is still lacking due to a limited understanding of the GDGT biosynthesis pathway (Jain *et al*., 2014), though a number of steps have recently come to light. The synthesis of GDGT core lipids involves the highly unsaturated intermediate, di-geranylgeranyl glycerol phosphate (DGGGP). Formation of GDGT-0 from two molecules of DGGGP requires donation of 28 electrons (14 e^- pairs), via geranylgeranyl reductase, (GGR) (Nishimura and Eguchi, 2006; Sasaki *et al*., 2011; Jain *et al*., 2014). It is possible that formation of the cyclopentyl rings precedes complete saturation of the double bonds (Zeng *et al*., 2019). Each ring formed reduces this demand by two electrons, providing a direct physiological link between available energy, the formation of cyclopentyl rings, and archaeal membrane lipid composition. The synthesis of ring-containing GDGTs decreases ion permeability; given the tight correlation here between specific growth rate and ring index—even when temperature and pH are invariant—supports *energy stress* as the unifying principle to all major environmental factors (temperature, pH, dissolved oxygen or electron donor availabilities) that are observationally correlated with changes in archaeal membrane composition (De Rosa *et al*., 1980; Gliozzi *et al*., 1983; van de Vossenberg *et al*., 1998; Uda *et al*., 2001; Uda *et al*., 2004; Boyd *et al*., 2013; Elling *et al*., 2015; Siliakus *et al*., 2017; Sollich *et al*., 2017). As previously suggested by others (Feyhl-Buska *et al*., 2016), the preferential synthesis of more highly cyclized GDGTs might represent a general physiological response to stress—whether thermal, pH or nutrient—across archaeal taxa.

Our results suggest that energy budgeting is the unifying concept that explains how different environmental variables influence archaeal lipid distribution and membrane properties. Higher temperatures are positively correlated with GDGT cyclization and ring index. Tighter lipid packing increases membrane integrity and reduces energy costs, allowing cells to cope with the higher rates

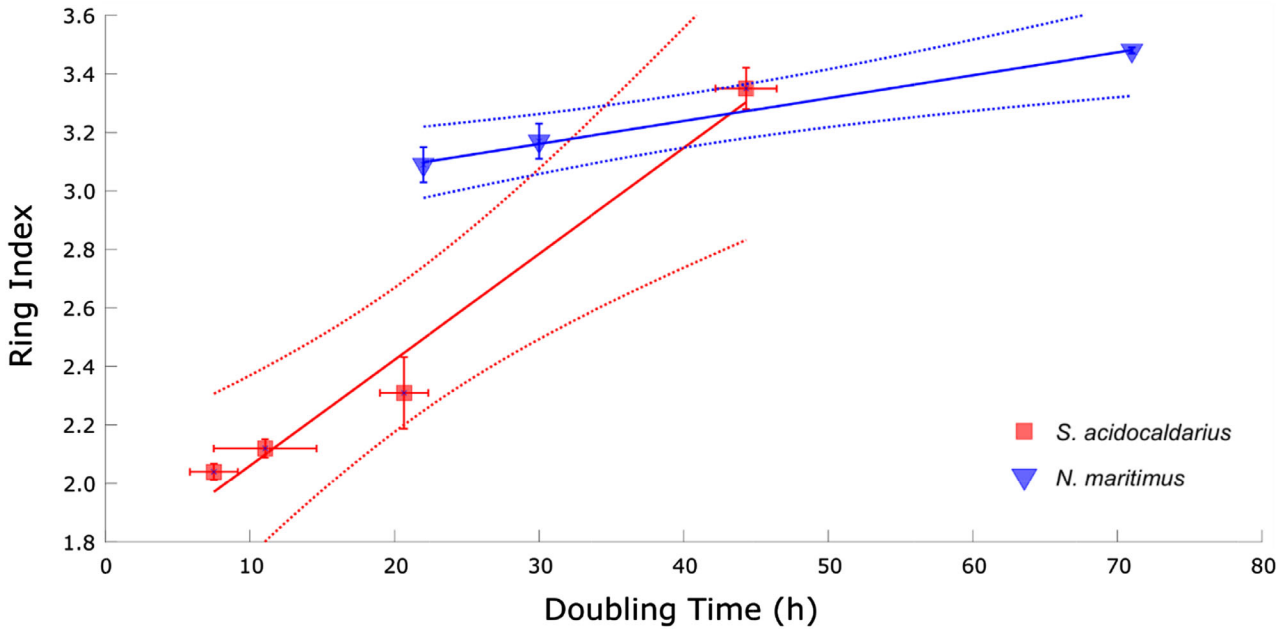

Fig. 6. Continuous culture experiments plotting doubling time versus ring index from *S. acidocaldarius* (R^2 = 0.98; p = 0.01; m = 0.036) relative to *N. maritimus* (R^2 = 0.99, p = 0.03; m = 0.008) in Hurley *et al*. (2016). Data from *S. acidocaldarius* are averaged across triplicate bioreactors for each growth rate versus a single reactor for *N. maritimus*. Dashed lines represent 95% confidence intervals.

of biomolecule turnover caused by thermal degradation. Similarly, the ability to decrease membrane permeability can help maintain optimal intracellular pH by minimizing proton leakage. Finally, cell populations in lag or stationary phase are nutrient- and energy-limited, and GDGT cyclization is doubly beneficial in that it reduces both electron demand and the spontaneous movement of solutes down their electrochemical gradient. Here we show that controlling nutrient and energy availability against a constant background of temperature and pH stress induces a significant change in GDGT compositions.

This finding has important ramifications for the interpretation of archaeal lipid distributions in the context of paleoenvironmental reconstructions. Changes in GDGT cyclization are more directly quantified by RI than by the TEX_{86} ratio. RI gives the average number of rings of an entire GDGT pool, whereas TEX_{86} expresses the abundance of GDGT-1 relative to the other cyclized GDGTs and was developed specifically to relate lipid distributions to sea surface temperatures (SSTs; Schouten *et al*., 2002; Schouten *et al*., 2007). Ideally, both RI and TEX_{86} would be reported in environmental calibrations or temperature reconstructions, given experimental evidence demonstrating that other factors independently influence GDGT cyclization (Boyd *et al*., 2011; Elling *et al*., 2014; Elling *et al*., 2015; Qin *et al*., 2015; Feyhl-Buska *et al*., 2016; Hurley *et al*., 2016). Preliminary work on the utility of RI as a complementary metric shows that coupling it with TEX_{86} can highlight when GDGT distributions are influenced by non-thermal factors or are behaving differently from average, modern marine communities (Zhang *et al*., 2016).

Current calibration functions of the TEX_{86} paleotemperature proxy systematically underestimate local SSTs in the tropics and overestimate them at the poles (Tierney, 2014). Given the results of this study and previous work documenting the effect of energy availability on RI and TEX_{86} (Elling *et al*., 2014; Qin *et al*., 2015; Hurley *et al*., 2016), we argue that these biases are likely introduced by temperature-independent environmental and ecological parameters. Marine Thaumarchaeota are ammonia oxidizers whose energy generation is dependent on oxygen as the terminal electron acceptor (Spang *et al*., 2010; Stahl and de la Torre, 2012). Persistent suboxia and anoxia are common features of modern and ancient restricted basins, such as the proto-Atlantic Ocean during the Cretaceous and Jurassic Oceanic Anoxic Events (Meyer and Kump, 2008). These environmental conditions may directly affect the metabolic activity of marine archaea and therefore impact the TEX_{86} signal in these regions and time intervals. For example, experiments have shown that restricting O_2 supply in batch cultures can result in as much as a 10°C increase in TEX_{86} temperature estimates in excess of experimental incubation temperature (Qin *et al*., 2015), and a similar shift of 6°C can be induced by altering the electron donor (ammonia) supply in chemostat cultures (Hurley *et al*., 2016). When the results from both distinct experimental approaches are normalized to the same reference frame, biases in TEX_{86} are explained by changes in growth rate and ammonia oxidation rate (Hurley *et al*., 2016). Our study confirms that energy availability can independently influence GDGT cyclization. It is therefore imperative to consider the effect of cellular bioenergetics on lipid distributions when interpreting sedimentary records from environments influenced by low O_2 concentrations or limited electron-donor availability.

For example, energy limitation may explain why TEX_{86}-inferred temperatures are anomalously warm (up to +12°C) in modern suboxic settings such as in the permanent oxygen minimum zones (OMZs) of the Eastern Tropical North Pacific Ocean and Arabian Sea, or in seasonally oxygen-deficient regions in coastal upwelling regimes (Schouten *et al*., 2012; Basse *et al*., 2014; Xie *et al*., 2014). In support of this hypothesis, sediments from the Murray Ridge seamount summit, which extends into the Arabian Sea OMZ, yield higher TEX_{86} temperatures than sediment from adjacent locations that lie below the OMZ (Lengger *et al*., 2012). Conversely, high energy availabilities are associated with cold biases both in controlled pure culture experiments (Elling *et al*., 2014; Hurley *et al*., 2016) and in natural settings such as high-nutrient upwelling systems (Lee *et al*., 2008). In such instances, high productivity and remineralization rates cause RI- and TEX_{86}-derived temperatures to drop below measured temperatures (Hurley *et al*., 2018).

Our study establishes that the heterotrophic thermoacidophile *S. acidocaldarius* exhibits a marked membrane-level response to changes in electron donor availability. These results provide an important experimental counterpart to continuous culture work with the mesophilic and chemoautotrophic archaeon *N. maritimus* (Hurley *et al*., 2016). In both studies, the energy available to cells was varied independent of temperature or pH by controlling the influx of substrates involved in metabolic redox reactions. Together, these experiments suggest that the denser membrane packing associated with core lipid cyclization is a mechanism that allows diverse GDGT-producing archaea to cope with energy stress. Quantifying the influence of cellular bioenergetics on archaeal membrane composition may allow for more complete interpretations of GDGT-based records from hot spring, soil, lake and marine settings. The recent identification of two enzymes required for pentacyclic ring formation in *S. acidocaldarius* (Zeng *et al*., 2019), will also further our understanding of GDGT-recorded responses to environmental conditions. Biomarker-based reconstructions of past environments can be improved by incorporating calibrations that account for local biogeochemical parameters relevant to archaeal energy metabolisms and subsequent membrane reordering.

Methods

Culturing conditions

Sulfolobus acidocaldarius DSM 639 was provided by Dr. S-V Albers (University of Freiburg, Germany), and cultured at 70 °C in complete Brock medium supplemented with 0.1% NZ-Amine and 0.2% sucrose (see *SI Materials and Methods*) at pH 2.25 (± 0.2). Initial cultures were grown at 70°C and 200 rpm (Innova-42 shaking incubators, Eppendorf). Three 1-L autoclavable glass bioreactors (Applikon, Delft, the Netherlands) were subsequently inoculated with 20 ml of a second-generation culture at mid-exponential phase to an initial optical density of 0.01 at 600 nm (OD_{600}).

The three bioreactors were operated in parallel under continuous culture conditions (see *SI Materials and Methods*; Supporting Information Fig. S2). Reactors were maintained at 70°C, stirred at 200 rpm (Rushton-type impeller), and aerated with a constant flux of 200 ml/min Zero Air (ultra-high purity, UHP). To reduce evaporative volume loss, excess gas was released through condensers in the reactor headplate. Reactor liquid volume was held constant at 500 ml by equalizing influent and effluent pump rates using a balance control loop (Applikon My-Control software). Temperature, dissolved oxygen, pH and balance readings were logged continuously using the Lucullus Process Information Management System interface (Applikon).

In four consecutive experiments, the flow rate of the influent and effluent medium was set to target four discrete specific growth rates, μ = 0.069, 0.039, 0.023 and 0.010 h^{-1}, corresponding to reactor turnover times of T_t = 10, 18, 30 and 70 h, respectively. Cell concentrations were monitored by optical density measurements at 600 nm, and coincident fluctuations in dilution rate and optical densities were then used to calculate growth rate and deviation from steady state.

Lipid analysis

Biomass collection was initiated after each bioreactor had operated at or within ±10% of steady state for three consecutive turnovers at a given growth rate (Supporting Information Figs S7 and S8). Following collection of effluent into cold traps placed on ice, four 50 ml aliquots from each trap were centrifuged at 3214 × *g* and 4°C for 30 min (Eppendorf 5810 R, S-4-104 rotor). The supernatant was decanted after centrifugation and cell pellets were stored at −80°C until ready for freeze-drying and lipid extraction. To determine whether prolonged effluent collection impacted lipid distributions, 10 ml aliquots were also pulled directly from bioreactors during all 70 h experiment sampling events. Aliquots were drawn out through a syringe port and then processed as above.

Core GDGTs were isolated from freeze-dried biomass by acid hydrolysis followed by ultrasonic solvent extraction (e.g., Schouten *et al*., 2007b; Becker *et al*., 2013; Weber *et al*., 2017). To this end, freeze-dried cell pellets representing 50 ml aliquots of cell culture were submerged in 3 N methanolic HCl (33% H_2O) for 3 h at 70 °C. After cooling, methyl-tert-butyl-ether (MTBE) was added to achieve a MTBE:methanol ratio of 1:1 (vol.), and the samples were agitated using a Qsonica Q500 ultrasonic probe (cup horn, maximum amplitude, 5 min total pulse time). Phase separation was induced by changing the solvent composition to MTBE:methanol:hexane (1:1:1, vol.), and the upper organic phase was collected after centrifugation. The total lipid extract (TLE) was subsequently dried under a flow of N_2 and stored at −20 °C in a solution of 1% isopropyl alcohol (IPA) in hexane until analysis. Given that calidol-headgroup lipids occur in *Sulfolobus* sp. but are resistant to extraction even with 3 N HCl, we focused this effort on the non-calditol core lipids.

Core GDGTs were analysed by ultra-high performance liquid chromatography—atmospheric pressure chemical ionization—mass spectrometry (UHPLC-APCI-MS) using an Agilent 1290 Infinity series UHPLC system coupled to an Agilent 6410 triple-quadrupole mass spectrometer (MS), operated in positive mode (gas temperature: 350 °C; vaporizer temperature: 300 °C; gas flow: 6 l min^{-1}, nebulizer pressure: 60 psi). Analytical separation of GDGTs was achieved by injecting 2–10 µl of the total lipid extract onto an array of two-coupled Acquity BEH HILIC amide columns (2.1 × 150 mm, 1.7 µm particle size, Waters, Eschborn, Germany) maintained at 50 °C and fitted with a pre-column of the same material. GDGTs were eluted using a linear gradient from 0.2% to 10% (vol.) IPA in hexane at a flow rate of 0.5 ml/min as previously described (39). At the end of each sample run, the columns were back-flushed with a 70:30 mixture of hexane:IPA (90:10, vol:vol) and IPA:methanol (70:30, vol:vol), and the columns were reequilibrated to initial condition. The MS was operated in single ion monitoring mode (dwell time 25 ms, fragmentor voltage: 75 V), and GDGTs were quantified by the integration of the ion chromatograms of m/z 1302.3 (GDGT-0), m/z 1300.3 (GDGT-1), and so forth. The ring index (RI) of GDGTs reflects the relative amount of cyclopentyl rings and is defined as: The *RI* metric compresses GDGT distributions into a

$$RI = \frac{1x[GDGT-1] + 2x[GDGT-2] + 3x[GDGT-3] + 4x[GDGT-4] + 5x[GDGT-5] + 6x[GDGT-6]}{[GDGT-0] + [GDGT-1] + [GDGT-2] + [GDGT-3] + [GDGT-4] + [GDGT-5] + [GDGT-6]} \quad (1)$$

single value representing the average number of cyclopentyl rings in GDGTs for each sample.

Growth rate and doubling time calculations

Cell densities were monitored at regular intervals throughout the experiment by measuring the absorbance at 600 nm (A600) of a 1 ml aliquot pulled directly from each bioreactor. Dilution rates and turnover times were calculated by measuring the volume of effluent pumped out of each reactor per collection interval.

The net rate of change in cell concentration (d*x*/d*t*) is a function of the rates of cell division and dilution by sterile medium:

$$dx/dt = \mu x - Dx \quad (2)$$

where x = concentration of cells, μ = specific growth rate of the organism, and D = dilution rate (Novick and Szilard, 1950; Herbert *et al*., 1956). At steady state, the population's specific growth rate (μ) is equal to the dilution rate (D), such that the concentration of cells does not change with time ($dx/dt = 0$). Deviation from theoretical steady-state are approximated by calculating the difference between μ and D. Dilution rate is determined by measuring the rate of liquid effluent outflow, and μ is then estimated from measured absorbance data using a rearranged form of Equation 2:

$$\mu = \frac{\frac{dx}{dt} + Dx}{x} \quad (3)$$

Here d*x*/d*t* is the change in A600 between two consecutive time points (i.e., ΔA600/Δt, in h^{-1}), D is calculated dilution rate (h^{-1}) over the time interval, and x is the measured A600 value at given time point. The value of μ then used to calculate doubling time:

$$\text{Doubling time} = \frac{\ln(2)}{\mu} \quad (4)$$

We control and measure both dilution rate and reactor turnover time along with the corresponding biologically relevant metrics, that is, the calculated specific growth rate and doubling time. At a theoretical steady state in a chemostat, the specific growth rate of a population exactly equals the reactor dilution rate: μ = D. In practice, however, small variances between μ and D can emerge due to the dynamical nature of the reactor system and/or the microbial populations. Deviations from steady state may be driven by transient fluctuations in the internal state of microorganisms, the delivery rate of nutrients, or both. The deviation from theoretical steady state is expressed in relative terms as:

$$\text{Deviation from steady-state}\,(\%) = \frac{\mu - D}{D} \times 100\%. \quad (5)$$

Percent deviation from an idealized steady state was calculated and recorded each time optical density measurements were taken.

Statistical analysis

A two-sample *t*-test was used to assess whether the mean RI associated with each growth rate is significantly different from the others (Supporting Information Fig. S4). In order to compare the relative abundances of core GDGT variants between samples, we computed a Euclidian distance matrix and visualized dissimilarities between samples by hierarchical clustering using an average linkage technique (Supporting Information Fig. S3). All statistical analysis was carried out in MATLAB R2019b; scripts and data files are available online at https://github.com/AliceZhou73/Chemostat-Paper—Code-and-Data-Files.

Acknowledgements

For financial support we thank the ACS-PRF DNI #57209-DNI2 (WDL/YW), the Walter & Constance Burke Fund at Dartmouth College (WDL) and the NASA Space Grant award #NNX15AH79H; Swiss National Science Foundation (YW); and the Gordon and Betty Moore Foundation and NSF-1702262 (AP/FJE). We thank the other members of the Leavitt and Pearson labs for thoughtful discussion and support.

References

Basse, A., Zhu, C., Versteegh, G.J.M., Fischer, G., Hinrichs, K.-W., and Mollenhauer, G. (2014) Distribution of intact and core tetraether lipids in water column profiles of suspended particulate matter off cape Blanc, NW Africa. *Org Geochem* **72**: 1–13.

Becker, K.W., Lipp, J.S., Zhu, C., Liu, X.-L., and Hinrichs, K.-U. (2013) An improved method for the analysis of archaeal and bacterial ether core lipids. *Org Geochem* **61**: 34–44.

Boyd, E.S., Pearson, A., Pi, Y., Li, W.-J., Zhang, Y.G., He, L., *et al*. (2011) Temperature and pH controls on glycerol dibiphytanyl glycerol tetraether lipid composition in the hyperthermophilic crenarchaeon *Acidolobus sulfurireducens*. *Extremophiles* **15**: 59–65.

Boyd, E.S., Hamilton, T.L., Wang, J., He, L., and Zhang, C. L. (2013) The role of tetraether lipid composition in the adaptation of thermophilic archaea to acidity. *Front Microbiol* **4**: 62.

Bradley, J.A., Amend, J.P., and LaRowe, D.E. (2018) Bioenergetic controls on microbial ecophysiology in marine sediments. *Front Microbiol* **9**: 180.

Elferink, M.G., de Wit, J.G., Driessen, A.J., and Konings, W. N. (1994) Stability and proton-permeability of liposomes composed of archaeal tetraether lipids. *Biochim Biophys Acta* **1193**: 247–254.

Elling, F.J., Könneke, M., Lipp, J.S., Becker, K.W., Gagen, E.J., and Hinrichs, K.U. (2014) Effects of growth phase on the membrane lipid composition of the thaumarchaeon *Nitrosopumilus maritimus* and their implications for archaeal lipid distributions in the marine environment. *Geochim Cosmochim Acta* **141**: 579–597.

Elling, F.J., Könneke, M., Mußmann, M., Greve, A., and Hinrichs, K.-U. (2015) Influence of temperature, pH, and salinity on membrane lipid composition and TEX_{86} of marine planktonic thaumarchaeal isolates. *Geochimica et Cosmochim Acta* **171**: 238–255.

Feyhl-Buska, J., Chen, Y., Jia, C., Wang, J.-X., Zhang, C.L., and Boyd, E.S. (2016) Influence of growth phase, pH, and temperature on the abundance and composition of tetraether lipids in the thermoacidophile *P. torridus*. *Front Microbiol* **7**: 1332.

Gabriel, J.L., and Chong, P.L.G. (2000) Molecular modeling of archaebacterial bipolar tetraether lipid membranes. *Chem Phys Lipids* **105**: 193–200.

Gliozzi, A., Paoli, G., De Rosa, M., and Gambacorta, A. (1983) Effect of isoprenoid cyclization on the transition temperature of lipids in thermophilic archaebacteria. *Biochim Biophys Acta* **735**: 234–242.

Herbert, D., Elsworth, R., and Telling, R.C. (1956) The continuous culture of bacteria; a theoretical and experimental study. *J Gen Microbiol* **14**: 601–622.

Hopmans, E.C., Schouten, S., Pancost, R.D., van der Meer, M.T. J., and Sinninghe-Damsté, J.S. (2000) Analysis of intact tetraether lipids in archaeal cell material and sediments by high performance liquid chromatography/atmospheric pressure chemical ionization mass spectrometry. *Rapid Commun Mass Spectrom* **14**: 585–589.

Hulbert, A.J., and Else, P.L. (2005) Membranes and the setting of energy demand. *J Exp Biol* **208**: 1593–1599.

Hurley, S.J., Elling, F.J., Könneke, M., Buchwald, C., Wankel, S.D., Santoro, A.E., *et al*. (2016) Influence of ammonia oxidation rate on thaumarchaeal lipid composition and the TEX_{86} temperature proxy. *Proc Natl Acad Sci* **113**: 7762–7677.

Hurley, S.J., Lipp, J.S., Close, H.G., Hinrichs, K.-U., and Pearson, A. (2018) Distribution and export of isoprenoid tetraether lipids in suspended particulate matter from the water column of the Western Atlantic Ocean. *Org Geochem* **116**: 90–102.

Jain, S., Caforio, A., and Driessen, A.J.M. (2014) Biosynthesis of archaeal membrane ether lipids. *Front Microbiol* **5**: 641.

Jarrel, H.C., Zukotynski, K.A., and Sprott, G.D. (1998) Lateral diffusion of the total polar lipids from *Thermoplasma acidophilum* in multilamellar liposomes. *Biochimica et Biophysica Acta—Biomembranes* **1369**: 259–266.

Jensen, S.M., Neesgaard, V.L., Skjoldbjerg, S.L.N., Brandl, M., Ejsing, C.S., and Treusch, A.H. (2015) The effects of temperature and growth phase on the lipidomes of *Sulfolobus icelandicus* and *Sulfolobus tokodaii*. *Life (Basel)* **5**: 1539–1566.

Kates, M. (1993) The biochemistry of Archaea (Archaebacteria). In *Membrane Lipids of Archaea*, Kushner, D.J., and Matheson, A.T. (eds). Amsterdam, Netherlands: Elsevier Science, pp. 261–295.

Koga, Y., and Morii, H. (2007) Biosynthesis of ether-type polar lipids in archaea and evolutionary considerations. *Microbiol Mol Biol Rev* **71**: 97–120.

Konings, W.N., Albers, S.V., Koning, S., and Driessen, A.J. M. (2002) The cell membrane plays a crucial role in survival of bacteria and archaea in extreme environments. *Antonie Van Leeuwenhoek* **81**: 61–72.

Lee, K.E., Kim, J.-H., Wilke, I., Helmke, P., and Schouten, S. (2008) A study of the alkenone, TEX_{86}, and planktonic foraminifera in the Benguela upwelling system: implications for past sea surface temperature estimates. *Geochemistry, Geophysics, Geosystems* **9**: Q10019.

Lengger, S.K., Hopmans, E.C., Reichart, G.-J., Nierop, K.G.J., Sinninghe-Damsté, J.S., and Schouten, S. (2012) Intact polar and core glycerol dibiphytanyl glycerol tetraether lipids in the Arabian Sea oxygen minimum zone: II. Selective preservation and degradation in sediments and consequences for the TEX_{86}. *Geochim Cosmochim Acta* **98**: 244–258.

Macalady, J.L., Vestling, M.M., Baumler, D., Boekelheide, N., Kaspar, C.W., and Banfield, J.F. (2004) Tetraether-linked membrane monolayers in *Ferroplasma* spp: a key to survival in acid. *Extremophiles* **8**: 411–419.

Meyer, K.M., and Kump, L.R. (2008) Oceanic euxinia in earth history: causes and consequences. *Annu Rev Earth Planet Sci* **36**: 251–288.

Nicolas, J.P. (2005) A molecular dynamics study of an archaeal tetraether lipid membrane: comparison with a dipalmitoylphosphatidylcholine lipid bilayer. *Lipids* **40**: 1023–1030.

Nishimura, Y., and Eguchi, T. (2006) Biosynthesis of archaeal membrane lipids: Digeranylgeranylglycerophospholipid reductase of the thermoacidophilic archaeon *Thermoplasma acidophilum*. *The Journal of Biochemistry* **139**: 1073–1081.

Novick, A., and Szilard, L. (1950) Description of the chemostat. *Science* **15**: 715–716.

Oger, P.M., and Cario, A. (2013) Adaptation of the membrane in Archaea. *Biophys Chem* **183**: 42–56.

Pearson, E.J., Juggins, S., Talbot, H.M., Weckström, J., Rosén, P., Ryves, D.B., *et al*. (2011) A lacustrine GDGT-temperature calibration from the Scandinavian Arctic to Antarctic: renewed potential for the application of GDGT paleothermometry in lakes. *Geochim Cosmochim Acta* **75**: 6225–6238.

Pineda De Castro, L.F., Dopson, M., and Friedman, R. (2016) Biological membranes in extreme conditions: simulations of anionic archaeal tetraether lipid membranes. *PLoS One* **11**: e0155287.

Powers, L., Werne, J.P., Vanderwoude, A.J., Sinninghe Damsté, J.S., Hopmans, E.C., and Schouten, S. (2010) Applicability and calibration of the TEX_{86} paleothermometer in lakes. *Org Geochem* **41**: 404–413.

Qin, W., Carlson, L.T., Armbrust, E.V., Devol, A.H., Moffett, J.W., Stahl, D.A., and Ingalls, A.E. (2015) Confounding effects of oxygen and temperature on the TEX_{86} signature of marine Thaumarchaeota. *Proceedings of the National Academy of Sciences USA* **112**: 10979–10984.

de Rosa, M., Gambacorta, A., Minale, L., and Bu'Lock, J. (1974) Cyclic diether lipids from very thermophilic acidophilic bacteria. *J Chem Soc Chem Commun* **14**: 543–544.

de Rosa, M., Esposito, E., Gambacorta, A., Nicolaus, B., and Bu'Lock, J.D. (1980) Effects of temperature on ether lipid composition of *Caldariella acidophila*. *Phytochemistry* **19**: 827–831.

Sasaki, D., Fujihashi, M., Iwata, Y., Murakami, M., Yoshimura, T., Hemmi, H., and Miki, K. (2011) Structure

and mutation analysis of archaeal geranylgeranyl reductase. *J Mol Biol* **409**: 543–557.

Schouten, S., Hopmans, E.C., Schefuβ, E., and Sinninghe Damsté, J.S. (2002) Distributional variations in marine crenarchaeotal membrane lipids: a new tool for reconstructing ancient sea water temperatures? *Earth Planet Sci Lett* **204**: 265–274.

Schouten, S., Forster, A., Panoto, F.E., and Sinninghe Damsté, J.S. (2007a) Towards calibration of the TEX_{86} paleothermometer for tropical sea surface temperatures in ancient greenhouse worlds. *Org Geochem* **38**: 1537–1546.

Schouten, S., Huguet, C., Hopmans, E.C., Kienhuis, M.V. M., and Sinninghe Damsté, J.S. (2007b) Analytical methodology for TEX_{86} paleothermometry by high-performance liquid chromatograph/atmospheric pressure chemical ionization-mass spectrometry. *Anal Chem* **79**: 2940–2944.

Schouten, S., Pitcher, A., Hopmans, E.C., Villanueva, L., Bleijswijk, J., and Sinninghe-Damsté, J.S. (2012) Intact polar and core glycerol dibiphytanyl glycerol tetraether lipids in the Arabian Sea oxygen minimum zone: I. selective preservation and degradation in the water column and consequences for the TEX_{86}. *Geochim Cosmochim Acta* **98**: 228–243.

Shinoda, K., Shinoda, W., Baba, T., and Mikami, M. (2007a) Molecular dynamics study of bipolar tetraether lipid membranes. *Biophys J* **89**: 3195–3202.

Shinoda, K., Shinoda, W., and Mikami, M. (2007b) Molecular dynamics simulation of an archaeal lipid bilayer with sodium chloride. *Phys Chem Chem Phys* **9**: 643–650.

Siliakus, M.F., van der Oost, J., and Kengen, S.W.M. (2017) Adaptations of archaeal and bacterial membranes to variations in temperature, pH and pressure. *Extremophiles* **21**: 651–670.

Sinninghe Damsté, J.S., Hopmans, E.C., Schouten, S., Van Duin, A.C.T., and Geenevasen, J.A.J. (2002) Crenarchaeol: the characteristic core glycerol dibiphytanyl glycerol tetraether membrane lipid of cosmopolitan pelagic crenarchaeota. *J Lipid Res* **43**: 1641–1651.

Sinninghe Damsté, J.S., Rijpstra, W.I.C., Hopmans, E.C., Jung, M.-Y., Kim, J.-G., Rhee, S.-K., *et al*. (2012) Intact polar and core glycerol dibiphytanyl glycerol tetraether lipids of group I.1a and I.1b Thaumarchaeota in soil. *Appl Environ Biol* **78**: 6866–6874.

Sollich, M., Yoshinaga, M.Y., Häusler, S., Price, R.E., Hinrichs, K.-U., and Bühring, S.I. (2017) Heat stress dictates microbial lipid composition along a thermal gradient in marine sediments. *Front Microbiol* **8**: 1550.

Spang, A., Hatzenpichler, R., Brochier-Armanet, C., Rattei, T., Tischler, P., Spieck, E., *et al*. (2010) Distinct gene set in two different lineages of ammonia-oxidizing archaea supports the phylum Thaumarchaeota. *Trends Microbiol* **18**: 331–340.

Stahl, D.A., and de la Torre, J.R. (2012) Physiology and diversity of ammonia-oxidizing archaea. *Annu Rev Microbiol* **66**: 83–101.

Tierney, J.E. (2014) Biomarker-based inferences of past climate: the TEX_{86} paleotemperature proxy. In *Treatise on Geochemistry: Second Edition*, Vol. **12**. Amsterdam, Netherlands: Elsevier, pp. 379–393.

Uda, I., Sugai, A., Itoh, Y.H., and Itoh, T. (2001) Variation in molecular species of polar lipids from *Thermoplasma acidophilum* depends on growth temperature. *Lipids* **36**: 103–105.

Uda, I., Sugai, A., Itoh, Y.H., and Itoh, T. (2004) Variation in molecular species of core lipids from the order *Thermoplasmales* strains depends on the growth temperature. *J Oleo Sci* **53**: 399–404.

Valentine, D.L. (2007) Adaptations to energy stress dictate the ecology and evolution of the Archaea. *Nat Rev Microbiol* **5**: 316–323.

van de Vossenberg, J., Driessen, A.J.M., Zillig, W., and Konings, W.N. (1998) Bioenergetics and cytoplasmic membrane stability of the extremely acidophilic, thermophilic archaeon *Picrophilus oshimae*. *Extremophiles* **2**: 67–74.

Weber, Y., Sinninghe Damsté, J.S., Hopmans, E.C., Lehmann, M.F., and Niemann, H. (2017) Incomplete recovery of intact polar glycerol dialkyl glycerol tetraethers from lacustrine suspended biomass. *Limnology and Oceanography: Methods* **15**: 782–793.

Wuchter, C., Schouten, S., Coolen, M.J.L., and Sinninghe Damsté, J.S. (2004) Temperature-dependent variation in the distribution of tetraether membrane lipids of marine Crenarchaeota: implications for TEX_{86} paleothermometry. *Paleooceanography and Paleoclimatology* **19**: PA4028.

Xie, S.T., Liu, X.L., Schubotz, F., Wakeham, S.G., and Hinrichs, K.U. (2014) Distribution of glycerol ether lipids in the oxygen minimum zone of the eastern tropical North Pacific Ocean. *Org Geochem* **71**: 60–71.

Yamauchi, K., Doi, K., Yoshida, Y., and Kinoshita, M. (1993) Archaebacterial lipids: highly proton-impermeable membranes from 1,2-diphytanyl-sn-glycero-3-phosphocholine. *Biochim Biophys Acta* **1146**: 178–182.

Zeng, Z., Liu, X.-L., Wei, J.H., Summons, R.E., and Welander, P.V. (2018) Calditol-linked membrane lipids are required for acid tolerance in *Sulfolobus acidocaldarius*. *Proc Natl Acad Sci* **115**: 12932–12937.

Zeng, Z., Liu, X.-L., Farley, K.R., Wei, J.H., Metcalf, W.W., Summons, R.E., and Welander, P.V. (2019) GDGT cyclization proteins identify the dominant archaeal sources of tetraether lipids in the ocean. *Proc. Nat. Academy Sci.* **116**(45), 22505–22511. https://doi.org/10.1073/pnas.1909306116.

Zhang, Y.G., Pagani, M., and Wang, Z. (2016) Ring index: a new strategy to evaluate the integrity of TEX_{86} paleothermometry. *Paleoceanography* **31**: 220–232.

Supporting Information

Additional Supporting Information may be found in the online version of this article at the publisher's web-site:

Appendix S1. Supporting Information.